Journal of Materials and Engineering Structures

Research Paper

Parametric study of crack propagation under thermal shock using phase field method

Quy-Minh Vuong [a], Anh-Tu Tran [b], Minh-Quan Thai [c,]*, Yann Charles [a], Jia Li [a]

[a] *Université Sorbonne Paris Nord, Laboratoire des Sciences des Procédés et des Matériaux, LSPM, CNRS, UPR 3407, F-93430, Villetaneuse, France*

[b] *University of Science and Technology of Hanoi, Vietnam Academy of Science and Technology, Hanoi, Vietnam*

[c] *University of Transport and Communications, 3 Cau Giay, Lang thuong, Dong Da, Hanoi, Vietnam*

ARTICLE INFO

Article history:

Received : 10 November 2024

Revised : 22 December 2024

Accepted : 28 December 2024

Keywords:

Thermal shock

Ceramics

Fracture

Phase-field modeling

ABSTRACT

Thermal shock is a major concern for brittle and quasi-brittle construction materials such as ceramics as it can easily lead to fracture. The complex mechanism and fracture pattern of this phenomenon make its analysis and prediction challenging. The phase-field method in this context is a promising candidate for simulating this phenomenon. By representing a discrete crack with a continuous damage variable that evolves according to its governing equations, the entire fracture process could be captured within the original finite element mesh. In this work, we developed a phase-field thermomechanical fracture model and implemented it into Abaqus software to reproduce literature work on the fracture behavior of ceramic materials subjected to water quenching. Different types of ceramic plates at various temperature conditions were investigated. The obtained results showed good agreement with the published works, validating the model implementation to be applied to further studies.

1 Introduction

Thanks to their versatility and high resistance to heat, corrosion and oxidation, ceramics materials have long been integral in civil engineering, with applications ranging from making tiles, bricks, glass to advanced construction materials and structural components [1]. However, their inherent brittleness make them susceptible to fracture under mechanical stress or sudden temperature change. This phenomenon is referred to as thermal shock, and an understanding of this type of failure is crucial for expanding the application of ceramics in demanding environments. Experimental studies have been carried out to examine the effects of thermal shock on different material samples. Jiang et al. [2] were among the first to

* *Corresponding author. Tel.: +84 815 559 669.*
E-mail address: minhquan.thai@utc.edu.vn

e-ISSN: 2170-127X,

RESEARCH REVIEW of Sciences and Technologies

investigate this by testing thin rectangular ceramic specimens 50x10x1 mm^3 with temperature ranging from 300ºC to 600ºC. D. Li et al. [3] investigated how the position of water exposure affects the thermal shock behaviour by immersing samples of similar materials with dimensions of 40x6x4 mm^3 into water, causing an abrupt temperature shift from 310ºC. This is a significant finding that has served as a basis for comparison in many subsequent simulation studies. Meanwhile, Shao et al. [4] used the modern apparatus with a resolution of 1024 x 512 pixels, enables real-time observation of cracking under suddenly temperature difference of 280°C in sheets measuring 50x10x0.4 mm^3. Liu et al. [5] analysed the crack propagation in thin, round plates with the following dimensions of 6.5-mm radius and 1 mm thickness subjected to a maximum temperature of 500°C before water immersion. Recently, Schlacher et al. [6] tested ceramic composites under thermal shocks with temperature differences between 200oC to 400oC, expanding insights into the durability of these engineered materials.

Besides theoretical and experimental investigation, numerical simulation has been widely adopted as it is a cost-effective tool. Different strategies have been proposed. In the lattice model [7], a homogeneous elastic material is modelled with a lattice approximation, crack propagation due to thermal shock is presented by a periodic sequence of temperature pulses with steep gradients. However, this model has limitations, as it assumes that the crack follow a straight path and moves at a constant speed. The model cannot solve the problem with cracks that follow a curve and move at a changing speed. Another approach, developed by Ricardo et al. [8], involves cohesive zone modeling (CZM) based on coupled energy and stress condition. This model enables the calculation of crack initiation time and length for a given crack spacing. However, to simplify the calculation, this model assumes material coefficients are temperature-independent, while in reality, these coefficients are more or less affected by temperature.

In recent years, the phase-field method has attracted increasing interest among fracture mechanics researchers. It originates from the pioneering works of Francfort and Marigo [9] for the theoretical foundation, and Bourdin et al. [10] for its numerical implementation. In this approach, the classic Griffith's theory of fracture mechanics [11] was reconsidered as the energy minimization problem. The discrete crack is replaced by a continuous damage variable ϕ, which evolves based on the constitutive equations. This method allows to capture complex fracture behavior such as crack nucleation [12], branching [13] and merging [14] without modifying the original finite element mesh. Thus, the method is therefore an excellent candidate to simulate thermal fracture in ceramics. Mandal et al. [15] performed an extensive study of the ceramics quenching test, in which the so-called BFGS algorithm is utilized to enhance the computational efficiency. However, as this work focused primarily on computational aspects, materials properties and boundary conditions were simplified, leading to some unrealistic damages patterns. On the other hands, Wang et al. [16] use the method to investigate surface cracking in ceramic bottles during rapid cooling. Like the previous study, this work also simplified thermal and material parameters, limiting the accuracy of results.

In this work, we present a phase-field model to analyze the thermal shock cracking behaviors of ceramics under water quenching in the software Abaqus. The model is adapted from the one presented in [17-22], extended for transient thermomechanical damage, and applied convective boundary conditions (BCs) instead of traditional Dirichlet BCs. Additionally, several materials parameters are treated as temperature-dependent to enhance the quality of the simulations. The results will be validated against experimental observations [2, 5] to evaluate the capabilities of the model to be applied in further context.

The remaining of the paper is organized as follow: Section 2 provides the background of the phase-field thermomechanical fracture model and the finite element implementation in Abaqus. Several benchmark examples are presented in Section 3, and relevant conclusions are drawn in the last section.

2 Method

Consider an n-dimensional body $\Omega \in \mathbb{R}^n$ $(n = \{1,2,3\})$ with surface $\partial\Omega \in \mathbb{R}^{n-1}$ and crack surface Γ, Ω/Γ representing the crack domain. For brittle fracture, the total energy of the system $\mathcal{E}$ is the sum of the strain energy and fracture energy, which can be written in variational form as:

$$\mathcal{E} = \int_{\Omega/\Gamma} \psi(\boldsymbol{u}) dV + \int_{\Gamma} G_c d\Gamma \tag{1}$$

where $\psi(\boldsymbol{u},T)$ is the volumetric strain energy,which is the function of the displacement and temperature fields $\boldsymbol{u}$ and T, while G_c represents the critical energy release rate as defined by Griffith [11]. In that context, the Γ's feature can be determined by minimizing $\mathcal{E}$ [7]. This task is computationally intractable due to the unknown nature of the sharp domain Γ. To overcome this, the domain is smeared out by introducing a continuous damage variable $\phi \in [0,1]$, which is equal to 0 outside the crack, and 1 at the crack location [23] (see Fig. 1). The level of smearing linked to a length scale l; when$l \to 0$, the sharp crack case is found [23].

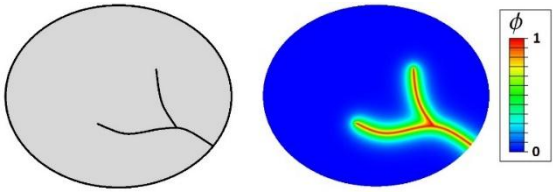

Fig. 1 – Example of sharp crack (left) and diffuse crack (right)

With ϕ and l, several models are developed to approximate equation (1), namely AT1 [22], AT2 [24] and phase-field cohesive zone model (PF-CZM) [17]. The AT1model features low regularization parameter, which effectively localizes the energy dissipation near the crack path, making it well-suited for brittle material [25]. Compare to AT1, the AT2 model introduces a smoother regularization term and spreads the fracture energy more diffusely, which makes it more versatile and can be applied to a wider range of materials. However, this model has less localization of the damage, which could impact the accuracy in case of sharp brittle fracture [12]. Meanwhile, the PF-CZM combines the advantages of phase-field modeling and cohesive zone mechanics, creating a more comprehensive approach for the initiation and propagation of cracks. However, its high computational complexity and requirements of careful parameter calibration could make this approach overly complicated [26].

In this problem, the fracture of ceramics materials can be assumed to be pure brittle, which makes AT1 the most suitable model. Following this model, equation (1) can be approximated as:

$$\mathcal{E} \approx \int_\Omega g(\phi)\psi_0(\boldsymbol{u},T)dV + \int_\Omega \frac{3G_c}{8l}(\phi + l^2|\boldsymbol{\nabla}\phi|^2)dV \tag{2}$$

where $\psi_0(\boldsymbol{u},T)$ is the volumetric strain energy of the undamaged material, $g(\phi)$ is the stress degradation function: $g(\phi) = (1-\phi)^2 + \kappa$ and κ is a very small number to prevent ill-condition[13]. The equation for the damage field ϕ evolution is the Euler-Lagrange equation of the functional $\mathcal{E}$ [23]:

$$g'(\phi)\psi_0(\boldsymbol{u},T) + \frac{3G_c}{8l}\left(1 - \frac{l^2\boldsymbol{\nabla}^2\phi}{2}\right) = 0 \tag{3}$$

The displacement field $\boldsymbol{u}$ is computed from the strain tensor $\boldsymbol{\varepsilon}$ and the Cauchy stress tensor $\boldsymbol{\sigma}$, assuming equilibrium:

$$\begin{cases} \varepsilon = \frac{1}{2}(\nabla u^{\mathrm{T}} + \nabla u) \\ \sigma = g(\phi)\frac{\partial\psi_0(u,T)}{\partial\varepsilon} \\ \nabla\cdot\sigma = 0 \quad \text{in } \Omega \end{cases} \tag{4}$$

The temperature field T, last, is obtained by modifying the heat transfer equation by accounting for the crack through the phase-field:

$$\rho C_p\dot{T} - \nabla.[g(\phi)k_0\nabla T] = r \tag{5}$$

where r is a heat source, k_0 is the thermal conductivity of undamaged material, ρ and C_p are the material density and specific heat, respectively. The thermal expansion is assumed to be isotropic, described by:

$$\varepsilon_T = \alpha\Delta T1 \tag{6}$$

where α is the thermal expansion coefficient, and **1** represents unit tensor in three dimensions.

To guarantee the damage irreversibility ($\dot{\phi} \geq 0$), a history variable H is introduced [23]:

$$H = \max_{\tau \in [0,t]} \psi_0^+ (\tau) \tag{7}$$

Equations (3), (4) and (5) can then be rewritten in a weak form:

$$\begin{cases} \int_\Omega \sigma : \delta\varepsilon dV = \int_{\partial\Omega_\sigma} \bar{T}.\delta u dS \\ \int_\Omega \left[\frac{3G_c}{8l}\left(1 - \frac{l^2\nabla^2\phi}{2}\right) - g'(\phi)H\right]\delta\phi dV = 0 \\ \int_\Omega \left[(\rho c\dot{T} - r)\delta T + g(\phi)k_0\nabla T.\delta\nabla T\right]dV = \int_{\partial\Omega_\sigma} \bar{T}.\delta u dS \end{cases} \tag{8}$$

in which $\partial\Omega_{\boldsymbol{\sigma}}$ (respectively $\partial\Omega_{\varphi n}$) is the part of $\partial\Omega$ where the stress $\overline{\boldsymbol{T}}$ (respectively normal heat flux $\bar{\varphi}_n$) is imposed, while $\partial\Omega_u$ and $\partial\Omega_T$ are the part of $\partial\Omega$ where displacement and temperature are imposed, respectively, with

$$\begin{cases} \partial\Omega = \partial\Omega_{\boldsymbol{\sigma}} \cup \partial\Omega_u \,\&\, \partial\Omega_{\boldsymbol{\sigma}} \cap \partial\Omega_u = \emptyset \\ \partial\Omega = \partial\Omega_{\varphi_n} \cup \partial\Omega_T \,\&\, \partial\Omega_{\varphi_n} \cap \partial\Omega_T = \emptyset \end{cases} \tag{9}$$

Last, $\delta\boldsymbol{u}$ and δT are continusous function which are equal to 0 on $\partial\Omega_u$ and $\partial\Omega_T$, respectively (with $\delta\boldsymbol{\varepsilon} = \frac{1}{2}(\delta\boldsymbol{u}^{\mathrm{T}} + \delta\boldsymbol{u})$. No such boundary conditions are needed for $\delta\phi$.

The system (8) is implemented in the Abaqus finite element software [27] by User Element (UEL) Subroutines [28]. Due to its flexibility, this subroutine was employed to implement coupled thermo-elastic-phase-field model, as outlined in Fig. 2.

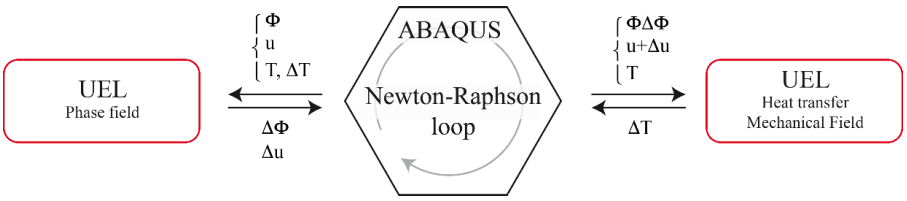

Fig. 2 – Flowchart of the Abaqus implementation of the coupled problem

In the staggered scheme, two different UELs are created: one for the coupled thermo-mechanic and other for the phase-field variable, both using four-node quadrilateral bilinear elements with Finite Element Method framework. The use of two UELs requires the creation of two element types in a layered configuration – one for thermo-mechanic, another for phase-field, and a "dummy" layer with no stiffness made from internal element which Abaqus can recognise to visualize nodal values of degrees of freedom (DoFs). These layers of elements are connected to each other by the same nodes, but with different DOFs. For each element, Abaqus provides the values of DOFs (displacements, temperature, phase-field) of previous time increment which will be interpolated into integration points then calculate the subsequent values of DOFs at actual time increment. Within each loop, the UEL for coupled thermo-mechanic is executed first to compute displacements and temperature, which are then transfered into the second UEL to calculate the phase-field. This phase-field data is ultimately stored in the "dummy" layer for visualization in Abaqus.

The process is repeated for each integration point in the element, after which Abaqus assembles the global system of equations. Using the UEL approach, the RHS and AMATRX must be coded and return to solver. Abaqus then employs the internal Newton-Raphson method to obtain the solution.

Details of the implementation can be found in the literature [17-21, 29].

3 Applications

3.1 Set up of the problems

The proposed model is used to simulate quenching tests of ceramics, as published in literature [2, 5]: samples are heated to high temperatures T_0 (300-600ºC), then dropped into a cold water bath of T_∞ = 15-20ºC. Cracking due to thermal shock is then observed. Two experimental studies will be referred: The work of Jiang et al. [2] with 50x10x1 mm^3 rectangular specimens (Fig. 3a), and the test of Liu et al. [5] using 6.5-mm radius circular plates of the same thickness (Fig. 3b), with the corresponding modelling works.

Based on symmetries, only half of the rectangular specimen and a quarter of a circular plate are modeled in the simulation.

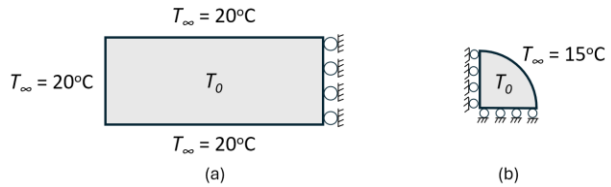

Fig. 3 – 2D geometry for simulation and boundary condition of the quenching tests of (a) rectangular specimen and (b) circular plate

In both works, the considered material is 99% purity alumina ceramics. The Poisson's ratio ν, Young's modulus E, critical energy release rate G_c, and the ultimate tensile stress σ_c are assumed to be temperature-independent in the range 15ºC – 600ºC (see Table 1); while the thermal conductivity k_0, specific heat C_p, thermal expansion coefficient α are considered to be temperature-dependent (see Table 2). Convective boundary conditions $\bar{\varphi}_n = h\Delta T$ are applied on the outer sample's surfaces, in which the convective heat transfer coefficient h is temperature-dependent [2, 5, 30].(see Table 2).

Table 1 - Temperature-independent material parameters of the studied ceramics [2, 5, 30]

E (GPa)	ν	G_c (J/m^2)	σ_c (MPa)
370	0.22	24.3	180

Table 2 - Temperature-dependent material parameters of the studied ceramics [2, 5, 30]

T_0 (ºC)	k_0 (W/(m.K))	C_p(J/(kg.K))	α(10^{-6}K^{-1})	h (kW/(m^2.K))
300	18	1150	7	54.5
350	15	1175	7.3	100
400	13	1200	7.5	86
500	11	1250	8	57
600	9	1270	8.5	45

From the graphs in original literature with data presented in Table 2, third-order polynomial fittings are applied to describe the variation of the material parameters due to temperature. In reference to the length scale $l$within the AT1 phase-field model, it is determined by [22]

$$l = \frac{3}{8}\frac{G_c E}{\sigma_c^2} \tag{10}$$

leading to l = 0.1 mm. To achieve reliable simulation, it is recommended to use a mesh size at least three times smaller than the length scale [17-21]. The rectangular specimen model is thus discretized into ~200 000 linear with full integration quad elements, and the circular plate with ~123 000 elements. The total simulation time is 0.2 s, which is divided into 2000 steps (with a staggered constant time increment).

3.2 Results & Discussion

3.2.1 Evolution of cracks

Fig. 4and gives the evolution of temperature T and the damage field ϕ, considering an initial temperature T_0 = 400ºC for the two experiments, at 3 moments: t = 0.0001s, at 0.1 s and at 0.2 s, respectively.

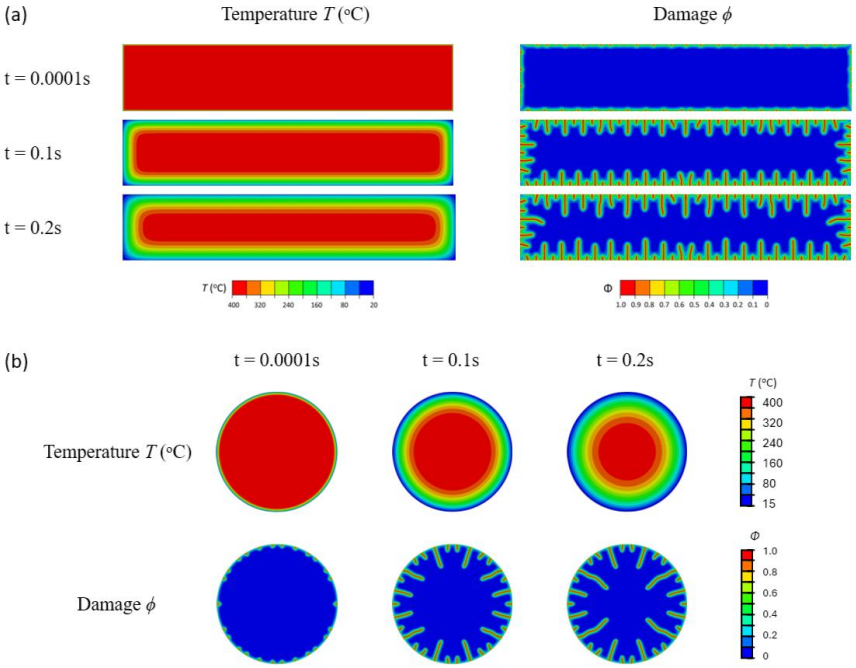

Fig. 4 – Evolution of temperature and fracture of the samples in the quenching test at T0 = 400oC: (a) Rectangular specimen and (b) Circular plate

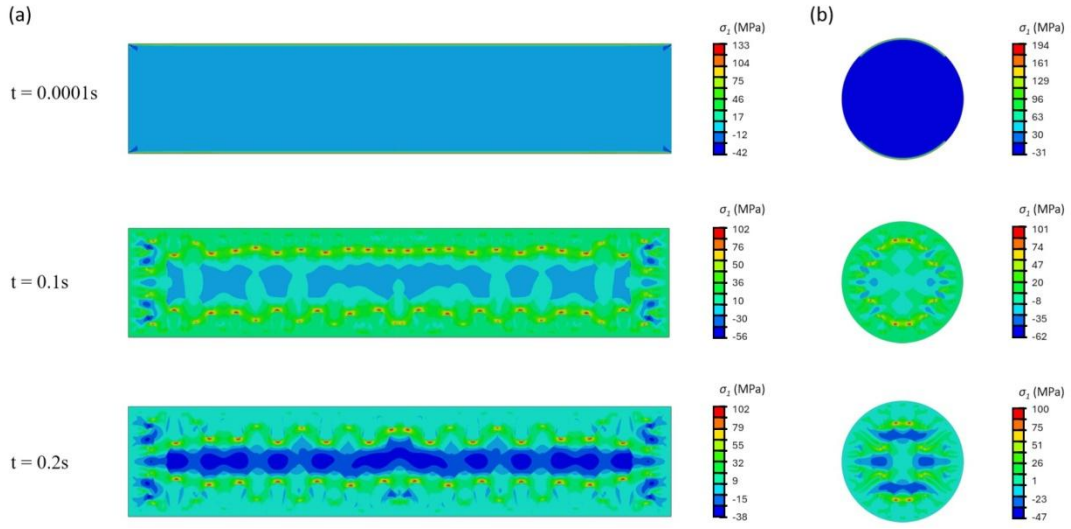

Fig. 5 – Evolution of maximum principal stress of the samples in the quenching test at T0 = 400oC: (a) Rectangular specimen and (b) Circular plate

The temperature profiles show a rapid cooling effect from the outer faces toward the center with steep thermal gradients, the red color indicating the hot part at 400ºC and the blue ones indicates ambient temperature (around 15–20ºC). This non-uniform temperature distribution induces significant thermal stresses, leading to fracture as illustrated by the damage field maps. The cracks initiate from the edges at the beginning (t = 0.0001 s), and propagate inward as seen at t =

0.1 s. At t = 0.2 s, as the cooling progress, the cracks continue to grow. Some cracks propagate further than others due to the lack of strain energy to support the growth of all the cracks simultaneously [31]. These evolution maps are similar to the one of Li et al. [32] using force-heat equivalence energy density principle, indicating the capability of the model to describe the relationship between temperature distribution and crack development.

To better understanding the temperature and fracture patterns, the evolution of maximum principal stress is shown in Fig. 5. Cracks initiate early in the process, influencing the stress distribution across the specimen. As crack evolution progresses, changes in the stress distribution as observed at t = 0.1s and t = 0.2s; once a crack forms, stress concentrates at its onset while stress relaxation is observed near the boundaries, progressively moving inward along the crack path. A compressive zone is formed over time at the middle of specimen that stops the crack evolution. The final crack path and shape depend strongly on the local competition between traction and compression which drive the crack growth.

3.2.2 Boundary conditions comparison

A contribution of this model is the application of convective boundary condition (BC) instead of traditional Dirichlet. As seen in Fig. 6, when Dirichlet BC is applied, the temperature constraint is fixed and the dissipation of heat is restricted, which results in unrealistic damage occuring along all edges of the samples. Meanwhile, the convective BC allows the temperature to vary along the edges and produces the pattern that aligns better with physical expectation. This highlights the importance of choosing the appropriate boundary condition, especially for the material that is highly sensitive to thermal gradients like ceramics.

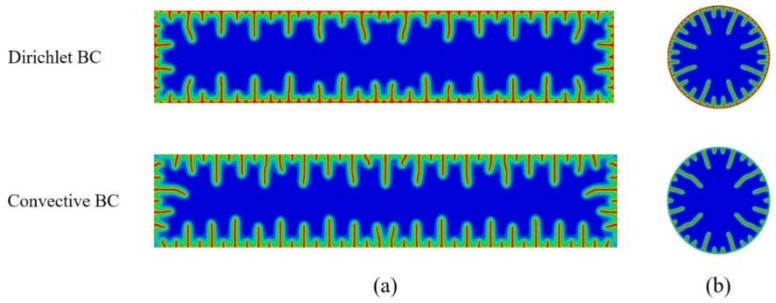

Fig. 6 – Comparison between Dirichlet and convective boundary conditions: (a) Rectangular specimen and (b) Circular plate

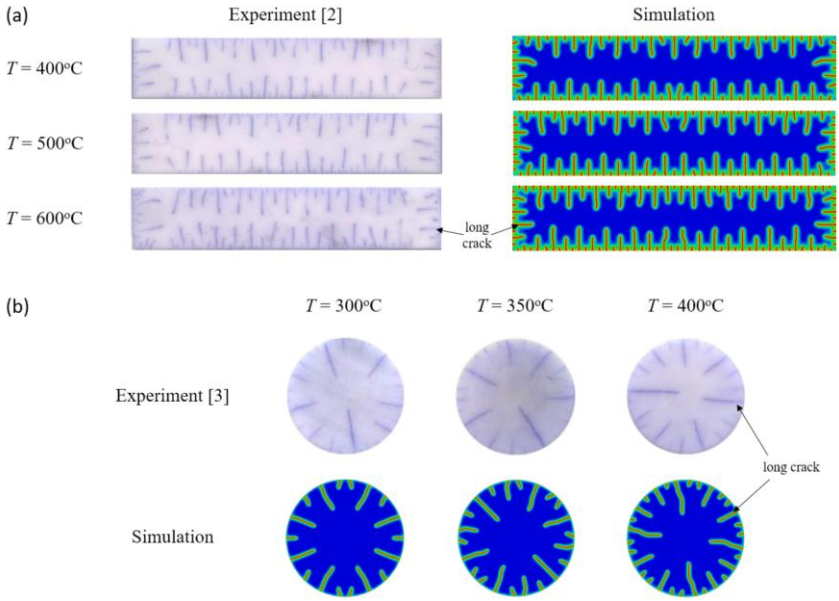

Fig. 7 – Comparison of simulation results with experimental investigations: (a) Rectangular specimen and (b) Circular plate

3.2.3 Validation with experiments

To validate the model, the simulated fracture patterns are compared with previously published studies (see Fig. 7 for comparison with experiments).

For the rectangular specimen (Fig. 7a), three simulations are performed at T_0 = 400ºC, 500ºC and 600ºC. The crack morphology shows a clear qualitative match with the experimental observations and fits with the already published works. On the edges one can observe multiple tiny cracks emerging, and a long crack typically appears after one or two short cracks, forming a quasi-periodic pattern. As the initial temperature rises, the number of cracks also increase, while the spacing between cracks decreases. Compared to the simulated results in [15] using Dirichlet BCs, the convective BCs in this work prevent the side-effect edge damage, giving more a realistic outcome.

Similar remarks could be drawn for the circular plate (Fig. 7b). Three simulations conducted at T_0 = 300ºC, 350ºC and 400ºC agrees well with the experimental results, from the radial crack pattern to the angular spacing between long cracks. The crack density and length increase with the temperature, with the 400ºC case showing the most extensive cracking.

The number of long cracks in all the cases are given in Table 3. The simulated values are slightly higher than the experimental ones, however the tendency is consistent. The difference can be explained by the simplification of the model: the material is assumed to be homogenous [32], and the affect of thermal stress on the variation of the damage ϕ is neglected [15].

Table 3 – Number of long cracks in both the simulation and experiment results

	Rectangular specimen			Circular plate		
	400ºC	**500ºC**	**600ºC**	**300ºC**	**350ºC**	**400ºC**
Experiment	36	40	42	7	8	10
Simulation	38	44	48	8	10	12

3.2.4 Investigation of crack initiation

With the model demonstrated to be robust, it is now applied to analyze crack initiation in two experimental setups. We track the maximum principal stress along the crack path before cracking process to justify this argument in two cases of geometries. The maximum principal stress at each point are shown in Fig. 8, where the x-axis represents the distance from the outer border to the point of interest, and the y-axis represents the maximum principal stress.

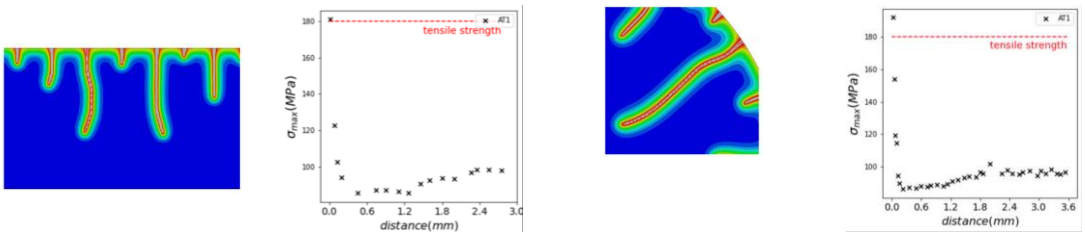

(a) (b)

Fig. 8 – Crack initiation investigation for (a) Rectangular specimen and (b) Circular plate

The results show that the stress approaches the material's strength near the crack initiation point. Once the crack begins to grow and develop, maximum stress observed before crack formation differs from that initiation point. This can be explained by the coupled criterion [33], which states that crack initiation at the vicinity of onset is driven by a stress criterion, while the propagation phase is governed by an energy criterion. This criterion can be used to explain the facts that maximum stress before cracking is lower than the material's strength and remains constant during propagation [12].

4 Conclusion

A coupled thermo-mechanic phase-field model is presented, to reproduce the fracture pattern observed in ceramics submitted to thermal shocks. It has been implemented into Abaqus via UEL Subroutines, allowing for the calculation and

identification of the locations of long cracks, as well as shorter cracks situated between them. The crack growth over time, starting from the moment of water contact and continuing in the following seconds, is clearly observed for cases where the parameters are both independent of and dependent on temperature, a task that is quite challenging to achieve in experimental studies. Moreover, the use of convective boundary condition allows the simulation to avoid damage at the border compared to that of Dirichlet boundary condition, which in turn makes the simulation more realistic. Investigation of crack initiation justifies the argument that AT1 model is suitable for simulating crack initiation in brittle materials. Indeed, as observed in stress state before crack, AT1 can well capture the initiation at material strength then crack will be driven by energy criterion in propagation phase. The presented results permit to reproduce both numerical and experimental results already published for this kind of application, allowing the validation of the implementation and its possible use on other configurations.

It is important to note that the AT1 model is suitable only for brittle material and not for quasi-brittle or others types of ductile fracture. The proposed model requires further development to improve its accuracy and efficiency and to expand its applicability to other thermally induced cases, for example impact of thermal shock from rapid cooling on the mechanical properties of concrete, or other multi-physics coupling problem. For instance, future work could be continued in order to integrate dynamic effects, extend the model to 3D structures and couple with other physical phenomenon.

Acknowledgements

This work has been carried out thanks to funding for Quy-Minh VUONG's PhD by the French Embassy in Vietnam through the France Excellence Scholarship Program (2022–2025).

REFERENCES

[1]- V.K. Chauhan, P. Thennarasu, R. Dubey, S. Pandey, R. Naresh, Recent efforts and advances towards sustainable ceramics made from textile wastes- A review. Open Ceramics, 16 (2023) 100500. doi:10.1016/j.oceram.2023.100500.

[2]- C.P. Jiang, X.F. Wu, J. Li, F. Song, Y.F. Shao, X.H. Xu, P. Yan, A study of the mechanism of formation and numerical simulations of crack patterns in ceramics subjected to thermal shock. Acta Materialia, 60(11) (2012) 4540-4550. doi:10.1016/j.actamat.2012.05.020.

[3]- D. Li, W. Li, R. Wang, D. Fang, The Effects of Water Entry Postures on the Thermal Shock Behavior of Alumina. International Journal of Applied Ceramic Technology, 13(1) (2016) 56-60. doi:10.1111/ijac.12411.

[4]- Y. Shao, F. Song, B. Liu, W. Li, L. Li, C. Jiang, Observation of ceramic cracking during quenching. Journal of the American Ceramic Society, 100(2) (2017) 520-523. doi:10.1111/jace.14674.

[5]- Y. Liu, X. Wu, Q. Guo, C. Jiang, F. Song, J. Li, Experiments and numerical simulations of thermal shock crack patterns in thin circular ceramic specimens. Ceramics International, 41(1, Part B) (2015) 1107-1114. doi:10.1016/j.ceramint.2014.09.036.

[6]- J. Schlacher, S. Geier, M. Schwentenwein, R. Bermejo, Towards 3D-printed alumina-based multi-material components with enhanced thermal shock resistance. Journal of the European Ceramic Society, 44(4) (2024) 2294-2303. doi:10.1016/j.jeurceramsoc.2023.11.009.

[7]- G. Carta, I.S. Jones, M. Brun, N.V. Movchan, A.B. Movchan, Crack propagation induced by thermal shocks in structured media. International Journal of Solids and Structures, 50(18) (2013) 2725-2736. doi:10.1016/j.ijsolstr.2013.05.001.

[8]- L.F. Faria Ricardo, D. Leguillon, G. Parry, A. Doitrand, Modeling the thermal shock induced cracking in ceramics. Journal of the European Ceramic Society, 40(4) (2020) 1513-1521. doi:10.1016/j.jeurceramsoc.2019.11.071.

[9]- G.A. Francfort, J.J. Marigo, Revisiting brittle fracture as an energy minimization problem. Journal of the Mechanics and Physics of Solids, 46(8) (1998) 1319-1342. doi:10.1016/S0022-5096(98)00034-9.

[10]- B. Bourdin, G.A. Francfort, J.J. Marigo, Numerical experiments in revisited brittle fracture. Journal of the Mechanics and Physics of Solids, 48(4) (2000) 797-826. doi:10.1016/S0022-5096(99)00028-9.

[11]- A.A. Griffith, VI. The phenomena of rupture and flow in solids. Philosophical transactions of the royal society of london. Series A, containing papers of a mathematical or physical character, 221(582-593) (1921) 163-198. doi:10.1098/rsta.1921.0006.

[12]- G. Molnár, A. Doitrand, R. Estevez, A. Gravouil, Toughness or strength? Regularization in phase-field fracture explained by the coupled criterion. Theoretical and Applied Fracture Mechanics, 109 (2020) 102736. doi:10.1016/j.tafmec.2020.102736.

[13]- G. Molnár, A. Gravouil, 2D and 3D Abaqus implementation of a robust staggered phase-field solution for modeling brittle fracture. Finite Elements in Analysis and Design, 130 (2017) 27-38. doi:10.1016/j.finel.2017.03.002.

[14]- X. Zhuang, S. Zhou, G.D. Huynh, P. Areias, T. Rabczuk, Phase field modeling and computer implementation: A review. Engineering Fracture Mechanics, 262 (2022) 108234. doi:10.1016/j.engfracmech.2022.108234.

[15]- T.K. Mandal, V.P. Nguyen, J.-Y. Wu, C. Nguyen-Thanh, A. de Vaucorbeil, Fracture of thermo-elastic solids: Phase-field modeling and new results with an efficient monolithic solver. Computer Methods in Applied Mechanics and Engineering, 376 (2021) 113648. doi:10.1016/j.cma.2020.113648.

[16]- T. Wang, H. Han, Y. Wang, X. Ye, G. Huang, Z. Liu, Z. Zhuang, Simulation of crack patterns in quasi-brittle materials under thermal shock using phase field and cohesive zone models. Engineering Fracture Mechanics, 276 (2022) 108889. doi:10.1016/j.engfracmech.2022.108889.

[17]- J.-Y. Wu, A unified phase-field theory for the mechanics of damage and quasi-brittle failure. Journal of the Mechanics and Physics of Solids, 103 (2017) 72-99. doi:10.1016/j.jmps.2017.03.015.

[18]- J.-Y. Wu, A geometrically regularized gradient-damage model with energetic equivalence. Computer Methods in Applied Mechanics and Engineering, 328 (2018) 612-637. doi:10.1016/j.cma.2017.09.027.

[19]- J.-Y. Wu, V.P. Nguyen, A length scale insensitive phase-field damage model for brittle fracture. Journal of the Mechanics and Physics of Solids, 119 (2018) 20-42. doi:10.1016/j.jmps.2018.06.006.

[20]- J.-Y. Wu, Y. Huang, V.P. Nguyen, On the BFGS monolithic algorithm for the unified phase field damage theory. Computer Methods in Applied Mechanics and Engineering, 360 (2020) 112704. doi:10.1016/j.cma.2019.112704.

[21]- J.-Y. Wu, Y. Huang, Comprehensive implementations of phase-field damage models in Abaqus. Theoretical and Applied Fracture Mechanics, 106 (2020) 102440. doi:10.1016/j.tafmec.2019.102440.

[22]- K. Pham, H. Amor, J.-J. Marigo, C. Maurini, Gradient Damage Models and Their Use to Approximate Brittle Fracture. International Journal of Damage Mechanics, 20(4) (2011) 618-652. doi:10.1177/1056789510386852.

[23]- C. Miehe, F. Welschinger, M. Hofacker, Thermodynamically consistent phase-field models of fracture: Variational principles and multi-field FE implementations. International journal for numerical methods in engineering, 83(10) (2010) 1273-1311. doi:10.1002/nme.2861.

[24]- B. Bourdin, G.A. Francfort, J.-J. Marigo, The Variational Approach to Fracture. Journal of Elasticity, 91(1) (2008) 5-148. doi:10.1007/s10659-007-9107-3.

[25]- E. Tanné, T. Li, B. Bourdin, J.J. Marigo, C. Maurini, Crack nucleation in variational phase-field models of brittle fracture. Journal of the Mechanics and Physics of Solids, 110 (2018) 80-99. doi:10.1016/j.jmps.2017.09.006.

[26]- R. Bharali, Numerical Methods and Multi-Scale Modeling for Phase-Field Fracture-With Applications in Linear Elastic and Poro-Elastic Media. Chalmers Tekniska Hogskola (Sweden), 2024.

[27]- Abaqus Analysis User's Guide, Simulia Inc., Providence, RI, USA. (2022).

[28]- Abaqus Analysis User Subroutines Reference Manual, Simulia Inc., Providence, RI, USA. (2022).

[29]- P. Le Grognec, E. Vasikaran, Y. Charles, P. Gilormini, Implementation of a reaction-diffusion process in the Abaqus finite element software. Mechanics & Industry, 21(5) (2020). doi:10.1051/meca/2020010.

[30]- J. Li, F. Song, C. Jiang, Direct numerical simulations on crack formation in ceramic materials under thermal shock by using a non-local fracture model. Journal of the European Ceramic Society, 33(13) (2013) 2677-2687. doi:10.1016/j.jeurceramsoc.2013.04.012.

[31]- H. Ruan, S. Rezaei, Y. Yang, D. Gross, B.-X. Xu, A thermo-mechanical phase-field fracture model: Application to hot cracking simulations in additive manufacturing. Journal of the Mechanics and Physics of Solids, 172 (2023) 105169. doi:10.1016/j.jmps.2022.105169.

[32]- D. Li, Y. Pang, T. Lu, Z. Liu, S. Chen, Numerical Analysis of Thermal Shock Cracking Behaviors of Ceramics Based on the Force-Heat Equivalence Energy Density Principle. Frontiers in Materials, 8 (2022). doi:10.3389/fmats.2021.825327.

[33]- D. Leguillon, Strength or toughness? A criterion for crack onset at a notch. European Journal of Mechanics - A/Solids, 21(1) (2002) 61-72. doi:10.1016/S0997-7538(01)01184-6.